

Evaluation of the CERN Super Proton Synchrotron longitudinal impedance from measurements of the quadrupole frequency shift

A. Lasheen^{1,2,*} and E. Shaposhnikova¹

¹CERN, CH-1211 Geneva, Switzerland

²Université Paris-Sud, 91400 Orsay, France

(Received 23 January 2017; published 13 June 2017)

Longitudinal instabilities are one of the main limitations in the CERN Super Proton Synchrotron (SPS) to reach the beam parameters required for the High Luminosity LHC project. In preparation to the SPS upgrade, possible remedies are studied by performing macroparticle simulations using the machine impedance model obtained from electromagnetic simulations and measurements. To benchmark the impedance model, the results of simulations are compared with various beam measurements. In this study, the reactive part of the impedance was probed by measuring the quadrupole frequency shift with intensity, obtained from bunch length oscillations at mismatched injection into the SPS. This method was applied over many last years to follow up the evolution of the SPS impedance, injecting bunches with the same bunch length. A novel approach, giving significantly more information, consists in varying the injected bunch length. The comparison of these measurements with macroparticle simulations allowed us to test the existing model, identify some missing SPS impedance and to obtain its possible dependence on frequency.

DOI: 10.1103/PhysRevAccelBeams.20.064401

I. INTRODUCTION

One of the main challenges for future physics projects relying on particle accelerators is the need for high beam intensity, which can be limited by different collective effects. The High Luminosity LHC (HL-LHC) project at CERN needs twice higher beam intensity than achieved so far [1]. The Super Proton Synchrotron (SPS) is the last accelerator of the LHC injector chain and is the main bottleneck in terms of intensity due to beam loading and longitudinal instabilities. As the required step in performance in the SPS is high, one of the goals of the LHC Injector Upgrade (LIU) project [2] is to identify the sources of this limitation and find solutions.

The instabilities are driven by the interaction of the beam with its environment. Changes in the vacuum chamber geometry lead to electromagnetic perturbations, modeled by a beam coupling impedance \mathcal{Z} . An accurate impedance model of the ring is needed to identify the most critical contribution. A survey of all elements in the machine has been done and their impedance was found using electromagnetic simulations and bench measurements. It includes now the contribution from most of the significant sources, such as the traveling wave rf cavities (TWC) and their

high-order modes (HOM), the injection/extraction kickers, the vacuum flanges (the biggest contributors correspond to the type near the focusing magnets QF), the pumping ports, and many other smaller sources [3,4]. At low energy in the SPS, longitudinal space charge ($\text{Im}\mathcal{Z}/n$)_{SC} is not negligible and needs to be correctly evaluated [5]. The present SPS impedance model is used in beam dynamics simulations and is presented in Fig. 1.

The comparison of beam measurements performed to probe the whole impedance with macroparticle simulations can give indications about the completeness of the impedance model. The reactive part of the machine impedance can be evaluated from the measurements of the synchrotron frequency shift with intensity. Various approaches were used in different accelerators. For example, the peak-detected Schottky (e.g., in the LHC [6]) and traditional Schottky signals (e.g., in the Relativistic Heavy Ion Collider [7]) can be used to directly observe the synchrotron frequency distribution, and the frequency shift is obtained by scanning the bunch intensity.

The method presented below relies on the measurements of bunch length oscillations at injection, initiated by a mismatched rf voltage. The frequency of these oscillations f_{s2} is approximately twice the linear synchrotron frequency and depends on the reactive part of the impedance as well as on the bunch intensity and length. Examples of recent measurements performed using bunches with different parameters are shown in Fig. 2.

The synchrotron frequency depends on the voltage seen by the beam, which is modified due to the voltage induced in the impedance sources. For bunches performing coherent

*alexandre.lasheen@cern.ch

Published by the American Physical Society under the terms of the Creative Commons Attribution 4.0 International license. Further distribution of this work must maintain attribution to the author(s) and the published article's title, journal citation, and DOI.

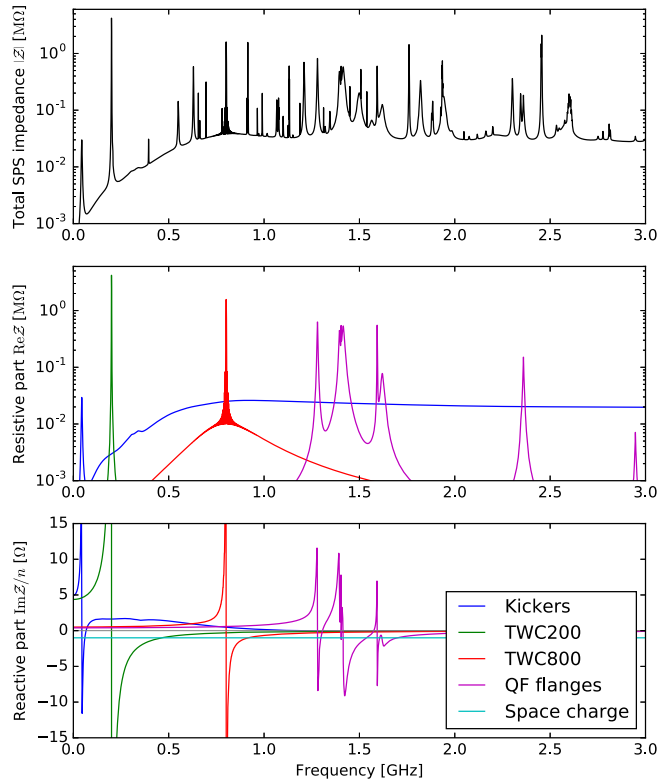


FIG. 1. The present SPS longitudinal impedance model (top: total absolute impedance, middle and bottom: resistive part and reactive part of the main contributions).

oscillations, the induced voltage contribution coming from the stationary part of the bunch distribution can be separated from the one coming from the mismatched part. The frequency of coherent oscillations can be presented in the following form [8]:

$$f_{s,m}(N_b) \approx m f_{s0} + m \Delta f_{\text{inc}}(N_b) + \Delta f_{\text{coh},m}(N_b), \quad (1)$$

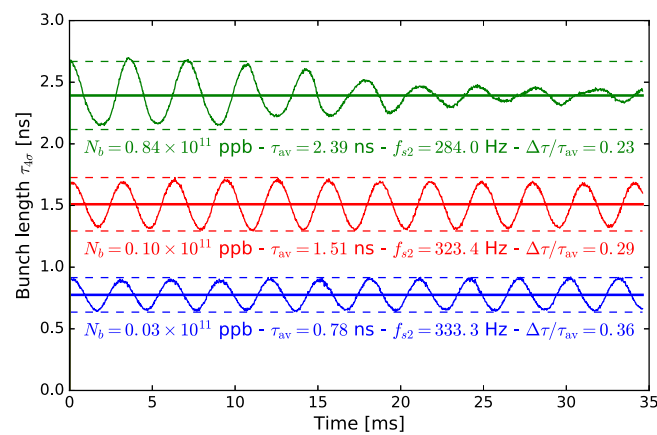


FIG. 2. Examples of bunch length oscillations at SPS injection measured in the Q26 optics for different average bunch lengths τ_{av} and intensities N_b .

where N_b is the bunch intensity (number of particles in the bunch ppb), m is the mode of the oscillations ($m = 1$ is dipole or bunch position oscillations, $m = 2$ is quadrupole or bunch length oscillations), f_{s0} is the synchrotron frequency for small amplitude of oscillations, Δf_{inc} is the incoherent frequency shift due to induced voltage from the stationary bunch distribution and $\Delta f_{\text{coh},m}$ the coherent frequency shift defined by the perturbation due to the mismatched part. For dipole oscillations, the coherent and the incoherent shifts are exactly compensating each other for a parabolic bunch (which is a common distribution for proton bunches in the SPS, see Sec. 6.4 in [9]), meaning that no information could be extracted so bunch length oscillations are used in this case.

Since 1999, this method was used to monitor the evolution of the SPS impedance as many pieces of equipment were shielded, removed, or installed [10]. The evolution of the measured quadrupole frequency shift with intensity is shown in Fig. 3 (represented by the slope b). In 1999, the main impedance contribution was from the pumping ports and the measured shift as a function of intensity was large ($b = -5.6$ Hz). The pumping ports were also the source of microwave instability in the SPS, a major limitation to reach the required beam parameters for the LHC. Therefore, their impedance was reduced by shielding in 2000. In 2001, the measured quadrupole frequency shift was lower ($b = -1.8$ Hz), proving that the impedance reduction was successful. The shift with intensity was measured several times between 2003 and 2007 after the installation of kicker magnets for extraction to the LHC (2003 and 2006), followed by their impedance reduction (2007). However, while the large changes were easy to see, the small variations in the quadrupole

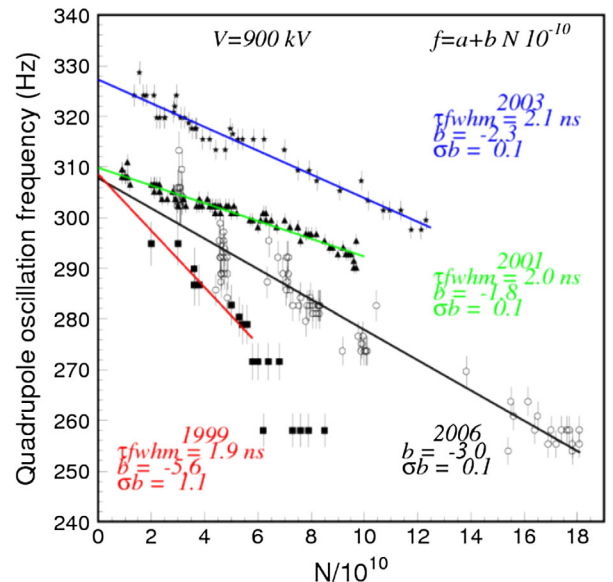


FIG. 3. Measurements of the quadrupole synchrotron frequency shift at 26 GeV/c in the SPS since 1999 [10].

frequency shift were difficult to measure. Studies showed that the measured shift b also strongly depends on the longitudinal emittance, and the lack of reproducibility in the average bunch length during measurements led to inconsistent results (e.g., the measured shift b increased in 2007, although the SPS impedance was reduced).

In this paper, measurements were extended to scanning both the bunch intensity and the average bunch length. We also demonstrate that the dependence on bunch length could even be used to extract additional information about the frequency characteristics of the impedance. To do so, we will first discuss the dependence of the synchrotron frequency shift on intensity and bunch length for quadrupole oscillations. Then, we will present the measurement method and results obtained for the two different SPS optics. Finally, measurements are compared with macro-particle simulations using the present SPS impedance model and deviations are exploited to estimate the remaining missing impedance.

II. QUADRUPOLE SYNCHROTRON FREQUENCY SHIFT

The bunch motion during quadrupole oscillations is shown in Fig. 4 in the $(\tau, \Delta E)$ phase space, where τ is the longitudinal coordinate of the particles and ΔE is the relative particle energy with respect to the beam total energy E . The measured bunch profile $\lambda(\tau)$ is the projection

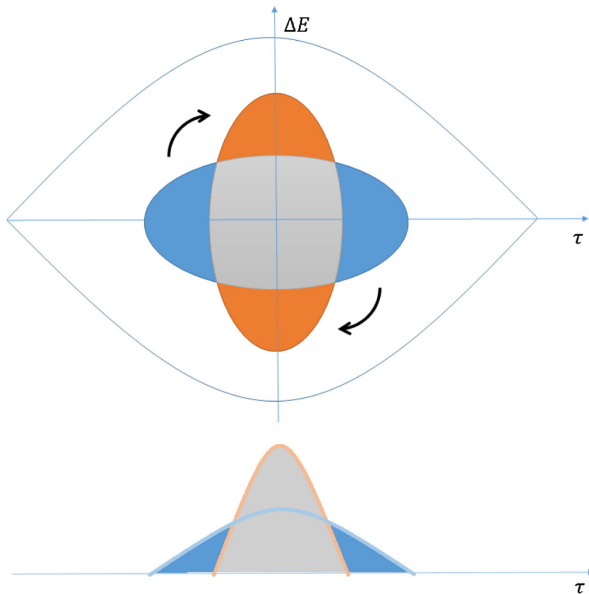


FIG. 4. Schematic presentation of the quadrupole oscillations. The upper figure represents the distribution in the phase space $(\tau, \Delta E)$, the lower one the corresponding longitudinal profile $\lambda(\tau)$, which is the projection of the bunch distribution in the τ dimension. The distribution is shown at two different times, in blue when the bunch length is the biggest and in orange when it is the smallest. The matched area (grey) does not contribute to the quadrupole oscillations, the mismatched area is in blue/orange.

of the bunch distribution in phase space on the τ coordinate. Two parts in the bunch distribution can be distinguished: the first one (in grey) corresponds to the matched area (or stationary part) of the bunch, and the second (blue/orange) to the mismatched part (or quadrupolar perturbation). Only the particles of the mismatched distribution are contributing to the measured quadrupole oscillations. In the absence of coherent oscillations (stable bunch), f_{s2} is defined by the frequency of the particles with the highest oscillation amplitude. Those are the ones that are the most affected by the nonlinearities of the rf bucket implying that the simplified expression in Eq. (1) which is usually derived for small amplitudes of oscillations may not be accurate anymore. In this section, we will consider the synchrotron frequency of the particles with large amplitude of oscillations.

A. Synchrotron frequency for particles with large oscillation amplitude

Let us first consider the quadrupole synchrotron frequency without intensity effects. For a particle oscillating in phase space with a maximum amplitude $\hat{\tau}$ in the τ dimension, the nonlinear synchrotron frequency $f_s^{(0)}(\hat{\tau})$ is [11]:

$$f_s^{(0)}(\hat{\tau}) = f_{s0} \frac{\pi}{2K[\sin(\omega_{\text{RF}}\hat{\tau}/2)]} \approx f_{s0} \left[1 - \frac{(\omega_{\text{RF}}\hat{\tau})^2}{16} \right], \quad (2)$$

where K is the complete elliptic integral of the first kind, ω_{RF} is the rf angular frequency, and f_{s0} is the synchrotron frequency for particles with small amplitude of oscillations ($\hat{\tau} \rightarrow 0$), defined as:

$$f_{s0} = \frac{1}{2\pi} \sqrt{\frac{\eta q V_{\text{RF}} \omega_{\text{RF}}}{\beta^2 E T_{\text{rev}}}}. \quad (3)$$

Here $\eta = \gamma_t^{-2} - \gamma^{-2}$ is the slippage factor, q is the particle charge, V_{RF} is the rf voltage, β is the relativistic factor corresponding to E and $T_{\text{rev}} = 1/f_{\text{rev}} = 2\pi/\omega_{\text{rev}}$ is the revolution period.

Without intensity effects, the synchrotron frequency $f_s^{(0)}$ has a quadratic dependence on the particle oscillation amplitude $\hat{\tau}$. We assumed above that the mismatched part of the bunch distribution is composed of particles with large amplitude of oscillations. For a small mismatch and assuming that the particles defining the mismatch have the same oscillation amplitude $\hat{\tau}$, we can replace in Eq. (2) $\hat{\tau} \approx \tau_L/2$, where τ_L is the full bunch length. Then, the quadrupole synchrotron frequency f_{s2} without intensity effects can be approximated as:

$$f_{s2}(\tau_L) \approx 2f_{s0} \left[1 - \frac{(\omega_{\text{RF}}\tau_L)^2}{64} \right]. \quad (4)$$

B. Incoherent synchrotron frequency shift

The effective voltage seen by a particle is modified by the induced voltage from all the impedance contributions along the ring. In this section, we will consider the modification of the synchrotron frequency distribution due to induced voltage from the stationary bunch distribution (incoherent shift Δf_{inc}). The induced voltage can be expressed as:

$$V_{\text{ind}}(\tau) = -qN_b \int_{-\infty}^{\infty} \mathcal{S}(f) \mathcal{Z}(f) e^{j2\pi f\tau} df \quad (5)$$

where $\mathcal{S}(f)$ is the bunch spectrum corresponding to the stationary part of the bunch distribution. A first approximation is found by considering particles with small amplitude of oscillations and expanding Eq. (5) up to the linear terms in τ , giving:

$$V_{\text{ind}}(\tau) \approx -qN_b f_{\text{rev}} (\mathcal{Z}_0 + \tau f_{\text{rev}} \mathcal{Z}_1). \quad (6)$$

The actual effect of the induced voltage on the bunch can be described by the effective resistive impedance \mathcal{Z}_0 and the effective reactive impedance \mathcal{Z}_1 , and are defined as [11]:

$$\mathcal{Z}_0 \underset{\hat{\tau} \rightarrow 0}{\approx} \frac{1}{f_{\text{rev}}} \int_{-\infty}^{\infty} \mathcal{S}(f) \text{Re} \mathcal{Z}(f) df, \quad (7)$$

$$\mathcal{Z}_1 \underset{\hat{\tau} \rightarrow 0}{\approx} -\frac{2\pi}{f_{\text{rev}}^2} \int_{-\infty}^{\infty} f \mathcal{S}(f) \text{Im} \mathcal{Z}(f) df. \quad (8)$$

The main effect of the effective resistive impedance \mathcal{Z}_0 is the asymmetry of the potential well and the synchronous phase shift. In the following development, the effect of \mathcal{Z}_0 on the synchrotron frequency shift is considered negligible. Therefore, the linear synchrotron frequency taking into account the induced voltage of a stationary bunch

distribution is affected by the effective reactive impedance \mathcal{Z}_1 as:

$$f_{s0,\text{inc}} = f_{s0} \sqrt{1 + \frac{q f_{\text{rev}}^2}{\omega_{\text{RF}} V_{\text{RF}}} \mathcal{Z}_1 N_b}. \quad (9)$$

To evaluate the effective reactive impedance \mathcal{Z}_1 , we discuss the relevant expressions of the bunch spectrum $\mathcal{S}(f)$ and the impedance $\mathcal{Z}(f)$ in the SPS. For proton bunches, the line density for a stationary distribution can be described using a binomial function:

$$\lambda(\tau) = \frac{2\Gamma(3/2 + \mu)}{\tau_L \sqrt{\pi} \Gamma(1 + \mu)} \left[1 - 4 \left(\frac{\tau}{\tau_L} \right)^2 \right]^\mu, \quad (10)$$

$$\lambda(|\tau| > \tau_L/2) = 0,$$

where the line density $\lambda(\tau)$ is normalized to 1 and $\Gamma(x)$ is the Gamma function. Below, we consider $\mu \geq 1$, with $\mu = 1$ giving a parabolic bunch and $\mu \rightarrow \infty$ a Gaussian bunch (typical values for the SPS bunches are in the range $\mu \in [1, 2]$). The rms bunch length of the distribution (10) is

$$\sigma_{\text{rms}} = \frac{\tau_L}{2\sqrt{3 + 2\mu}}. \quad (11)$$

Below, we will use the definition $\tau_{4\sigma} = 4\sigma_{\text{rms}}$ which is comparable to the full bunch length τ_L but is more convenient since for a fixed σ_{rms} , $\tau_L \rightarrow \infty$ if $\mu \rightarrow \infty$ ($\tau_{4\sigma}$ contains $\approx 95\%$ of the particles for $\mu \rightarrow \infty$ and 100% for $\mu = 1/2$). Moreover, the full bunch length τ_L is difficult to extract from measured profiles due to noise and it is not used for data analysis. Examples of bunch profiles are shown in Fig. 5(a) and the corresponding bunch spectra, shown in Fig. 5(b), have the form:

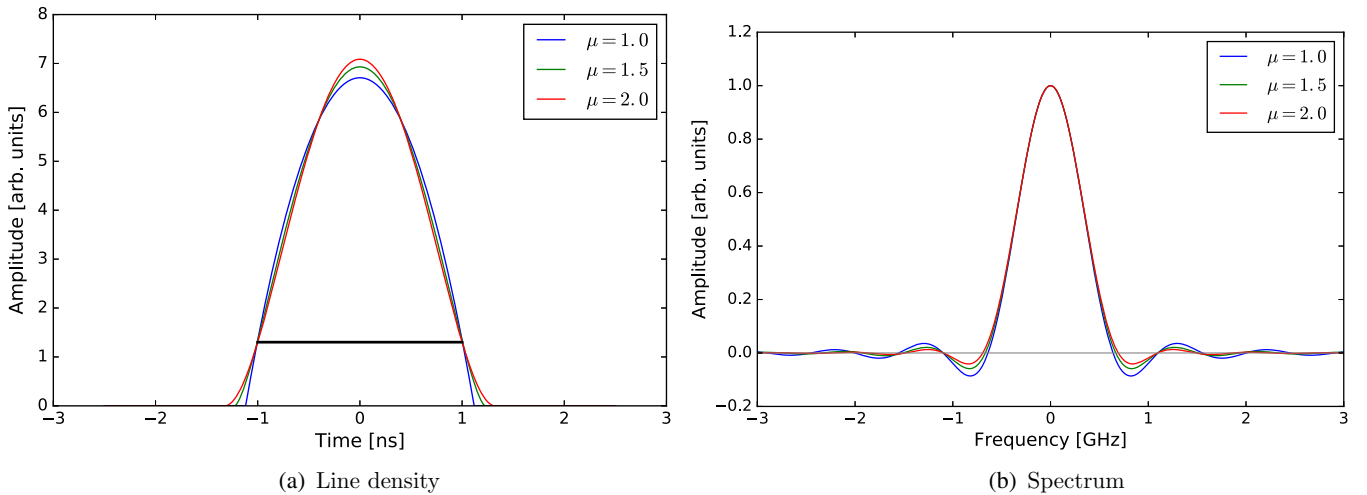


FIG. 5. Line densities (left) and corresponding spectra (right) for different μ values and the same rms bunch length σ_{rms} . The black line indicates the bunch length $\tau_{4\sigma}$.

$$\mathcal{S}(f) = {}_0F_1\left(\frac{3}{2} + \mu, -\frac{(\pi\tau_L f)^2}{4}\right), \quad (12)$$

where ${}_0F_1(x, y)$ is the Hypergeometric function.

In many practical cases, the impedance sources can be described as a resonator using the following expression:

$$\mathcal{Z}(f) = \frac{R}{1 + jQ\left(\frac{f}{f_r} - \frac{f_r}{f}\right)}, \quad (13)$$

where R is the shunt impedance, Q is the quality factor determining the decay time of the wake, and f_r is the resonant frequency. The contribution to the low frequency reactive impedance $\text{Im}\mathcal{Z}/n$, where $n = f/f_{\text{rev}}$, is

$$\frac{\text{Im}\mathcal{Z}}{n} \underset{f \rightarrow 0}{=} \frac{R f_{\text{rev}}}{Q f_r}. \quad (14)$$

Considering now a constant $\text{Im}\mathcal{Z}/n$ and using the bunch spectrum in (12) gives the analytical expression for \mathcal{Z}_1 :

$$\begin{aligned} \mathcal{Z}_1 &= -\frac{2\pi}{f_{\text{rev}}^3} \text{Im}\mathcal{Z}/n \int_{-\infty}^{\infty} f^2 \mathcal{S}(f) df \\ &= -\frac{8\Gamma(3/2 + \mu)}{\pi\sqrt{\pi}\Gamma(\mu)} \frac{\text{Im}\mathcal{Z}/n}{(f_{\text{rev}}\tau_L)^3}. \end{aligned} \quad (15)$$

The expression (9) for the linear synchrotron frequency valid for any μ is

$$f_{s0,\text{inc}} = f_{s0} \left[1 - \frac{16\Gamma(3/2 + \mu)q}{\sqrt{\pi}\Gamma(\mu)hV_{\text{RF}}\omega_{\text{rev}}^2} \frac{\text{Im}\mathcal{Z}/n}{\tau_L^3} N_b \right]^{\frac{1}{2}}, \quad (16)$$

where $h = \omega_{\text{RF}}/\omega_{\text{rev}}$ is the rf harmonic number. Assuming that the perturbation coming from the induced voltage is small and for a parabolic bunch ($\mu = 1$) the well-known formula for the incoherent synchrotron frequency shift is found back:

$$\frac{\Delta f_{\text{inc}}(\hat{\tau} \rightarrow 0)}{f_{s0}} \approx -\frac{6q}{hV_{\text{RF}}\omega_{\text{rev}}^2} \frac{\text{Im}\mathcal{Z}/n}{\tau_L^3} N_b. \quad (17)$$

Note that the incoherent synchrotron frequency shift has an inverse cubic dependence on bunch length, regardless of the bunch distribution (μ). Above transition, an inductive impedance ($\text{Im}\mathcal{Z}/n > 0$) decreases the linear synchrotron frequency, while a capacitive impedance ($\text{Im}\mathcal{Z}/n < 0$) increases it.

The expression for the incoherent synchrotron frequency shift in Eq. (16) is valid only for small amplitude of synchrotron oscillation. However the quadrupole oscillation frequency f_{s2} is determined by the particles with high amplitudes $\hat{\tau}$, as described in the previous section. It is not straightforward to express analytically Δf_{inc} for large $\hat{\tau}$. Moreover, for the usual bunch lengths the SPS impedance

cannot be well represented by a constant $\text{Im}\mathcal{Z}/n$ (which is also the case for most of the synchrotrons). For a resonant impedance (13), the reactive impedance $\text{Im}\mathcal{Z}$ is inductive for $f < f_r$ and capacitive for $f > f_r$. Hence, the effective impedance \mathcal{Z}_1 can be either inductive or capacitive depending on how the bunch spectrum overlaps with $\text{Im}\mathcal{Z}$. Note also the role of the positive and negative lobes in the bunch spectrum distribution [see Fig. 5(b)] that may change as well the value of the effective impedance \mathcal{Z}_1 .

The nonlinear incoherent synchrotron frequency shift can be calculated in the general case using the action-angle variables together with:

$$f_{s,\text{inc}}^{(0)}(\hat{\tau}) = \frac{1}{2\pi} \frac{d\mathcal{H}}{d\mathcal{J}}, \quad (18)$$

where \mathcal{H} is the Hamiltonian and \mathcal{J} is the action for a particle performing synchrotron oscillations with the amplitude $\hat{\tau}$. The nonlinear synchrotron frequency $f_{s,\text{inc}}^{(0)}$ was calculated numerically using Eq. (18) for different bunch profiles (μ) and bunch lengths $\tau_{4\sigma}$ taking into account the induced voltage. The SPS parameters for the Q26 optics in Table I were used, together with a simplified impedance model using $\text{Im}\mathcal{Z}/n = 3 \Omega$. An example is shown in Fig. 6 for $\tau_{4\sigma} = 0.7$ ns.

The relative incoherent synchrotron frequency shift $\Delta f_{\text{inc}}/f_s^{(0)}$ is presented in Fig. 7 as function of bunch length for small and large amplitude of particle oscillations (below, small amplitudes of particle oscillations correspond to $\hat{\tau} = 0$ and large amplitudes to $\hat{\tau} = \tau_{4\sigma}/2$). The expected scaling $\Delta f_{\text{inc}} \propto 1/\tau_L^3$ is in good agreement with the numerical results for both small and large amplitude of oscillations. We can then extend the Eq. (17) for any $\hat{\tau}$:

$$\frac{\Delta f_{\text{inc}}}{f_s^{(0)}}(\hat{\tau}) \approx -\frac{6q}{hV_{\text{RF}}\omega_{\text{rev}}^2} \frac{\text{Im}\mathcal{Z}/n}{\tau_L^3} N_b. \quad (19)$$

An interesting result is that the dependence on μ of the incoherent synchrotron frequency shift is bigger for $\hat{\tau} = 0$ than for $\hat{\tau} = \tau_{4\sigma}/2$. This is fortunate for the measurements since it implies that the measured quadrupole frequency f_{s2} should not depend too much on variations in the injected bunch profiles.

TABLE I. The SPS beam and machine parameters for the two different SPS optics at 26 GeV/c.

Optics	Transition gamma	rf voltage [MV]	Synchrotron frequency [Hz]	Bucket area [eVs]	Space charge $\left(\frac{\text{Im}\mathcal{Z}}{n}\right)_{\text{SC}}$ [Ω]
Q20	17.95	2.8	517.7	0.473	-1.0
Q26	22.77	0.9	172.4	0.456	-1.27

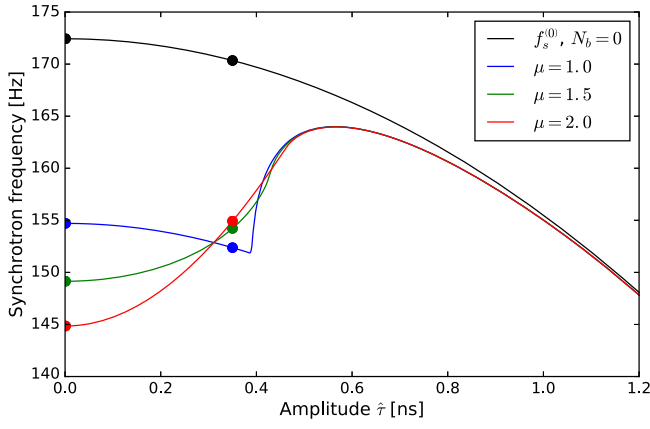


FIG. 6. The synchrotron frequency distribution $f_{s,\text{inc}}^{(0)}(\hat{\tau})$ for different values of μ with the same $\tau_{4\sigma} = 0.7$ ns, using a pure reactive impedance $\text{Im}\mathcal{Z}/n = 3\Omega$ and $N_b = 5 \times 10^{10}$ ppb for the Q26 optics parameters in Table I. The dots represents the values at $\hat{\tau} = 0$ and $\hat{\tau} = \tau_{4\sigma}/2$.

The same calculations were done using the full SPS impedance model with Eq. (18), and results are shown in Fig. 8(a) and 8(b). For particles with small amplitude of oscillations, the scaling $\propto 1/\tau_L^3$ does not work for the whole range of bunch lengths. Especially for very short bunches ($\tau_{4\sigma} < 0.7$ ns), where the longitudinal space charge impedance, which is capacitive, is dominant (see below the detailed contributions of different impedance sources). Moreover the dependence of the incoherent synchrotron frequency shift on bunch length is nonmonotonic. For particles with large amplitude of oscillations, the scaling $\propto 1/\tau_L^3$ is still relevant, with some variations due to the frequency structure of the SPS impedance. To evaluate how much the SPS impedance deviates from a constant reactive impedance, we define the equivalent impedance $(\text{Im}\mathcal{Z}/n)_{\text{eq}}$, based on Eq. (19), as:

$$(\text{Im}\mathcal{Z}/n)_{\text{eq}}^{\text{def}} = -\frac{\omega_{\text{rev}}^2 V_{\text{RF}} h \Delta f_{\text{inc}} \tau_{4\sigma}^3}{6q f_s^{(0)} N_b}. \quad (20)$$

This impedance corresponds to the reactive impedance required to get the incoherent synchrotron frequency shift Δf_{inc} , assuming a parabolic bunch. Note the use of the bunch length $\tau_{4\sigma}$ rather than τ_L , which is more convenient for the comparison with measurements in Sec. III.

The equivalent impedance $(\text{Im}\mathcal{Z}/n)_{\text{eq}}$ of the SPS for both small and large particle oscillation amplitudes $\hat{\tau}$ is shown in Fig. 8(c) and 8(d). For small $\hat{\tau}$, the deviation with respect to the expected scaling $\propto 1/\tau_L^3$ is significant and it is different in amplitude depending on the particle distribution μ . For instance, the equivalent impedance is $(\text{Im}\mathcal{Z}/n)_{\text{eq}} \approx 0$ for $\mu = 1$ and $\tau_{4\sigma} \approx 1.6$ ns, so that the synchrotron frequency shift is the same as if there are no intensity effects at all in the center of the bunch. For large $\hat{\tau}$, the shift also deviates from the expected scaling but with a different dependence on bunch length, indicating that the usual approximation of small particle oscillation amplitude $\hat{\tau} \rightarrow 0$ is not accurate. Additionally, a small variation of the average bunch length in measurements could lead to very different results meaning that the usual approximation of an impedance model with constant $\text{Im}\mathcal{Z}/n$ is also not an accurate representation. For example, measuring the quadrupole frequency shift for bunches with an average bunch length of $\tau_{\text{av}} \approx 1.4$ ns would give a bigger equivalent impedance than for $\tau_{\text{av}} \approx 1.7$ ns by $\approx 30\%$, as shown in Fig. 8(d).

Finally, the independent contribution of the main impedance sources in the SPS (shown in Fig. 1) taken separately was calculated. Their equivalent impedances $(\text{Im}\mathcal{Z}/n)_{\text{eq}}$ are shown in Fig. 9. These results are not directly comparable to the results obtained using the full impedance model since the contributions are not adding up linearly, but they give a rough estimation of what kind of shift can be

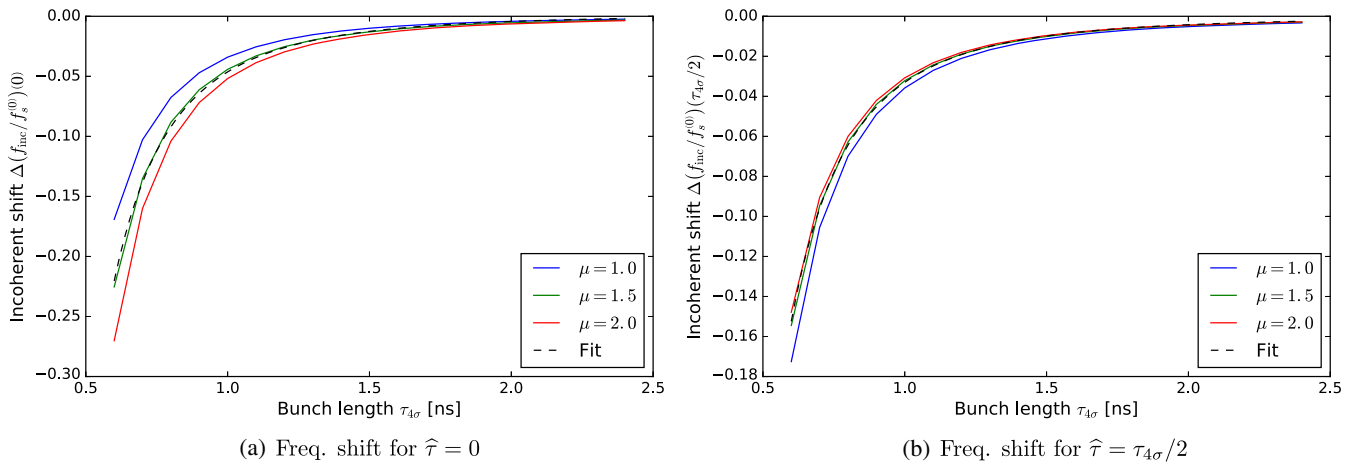


FIG. 7. The relative incoherent synchrotron frequency shift as a function of bunch length for particles with $\hat{\tau} \approx 0$ (left) and $\hat{\tau} = \tau_{4\sigma}/2$ (right), using a pure reactive impedance $\text{Im}\mathcal{Z}/n = 3\Omega$ and $N_b = 5 \times 10^{10}$ ppb for the Q26 optics parameters in Table I.

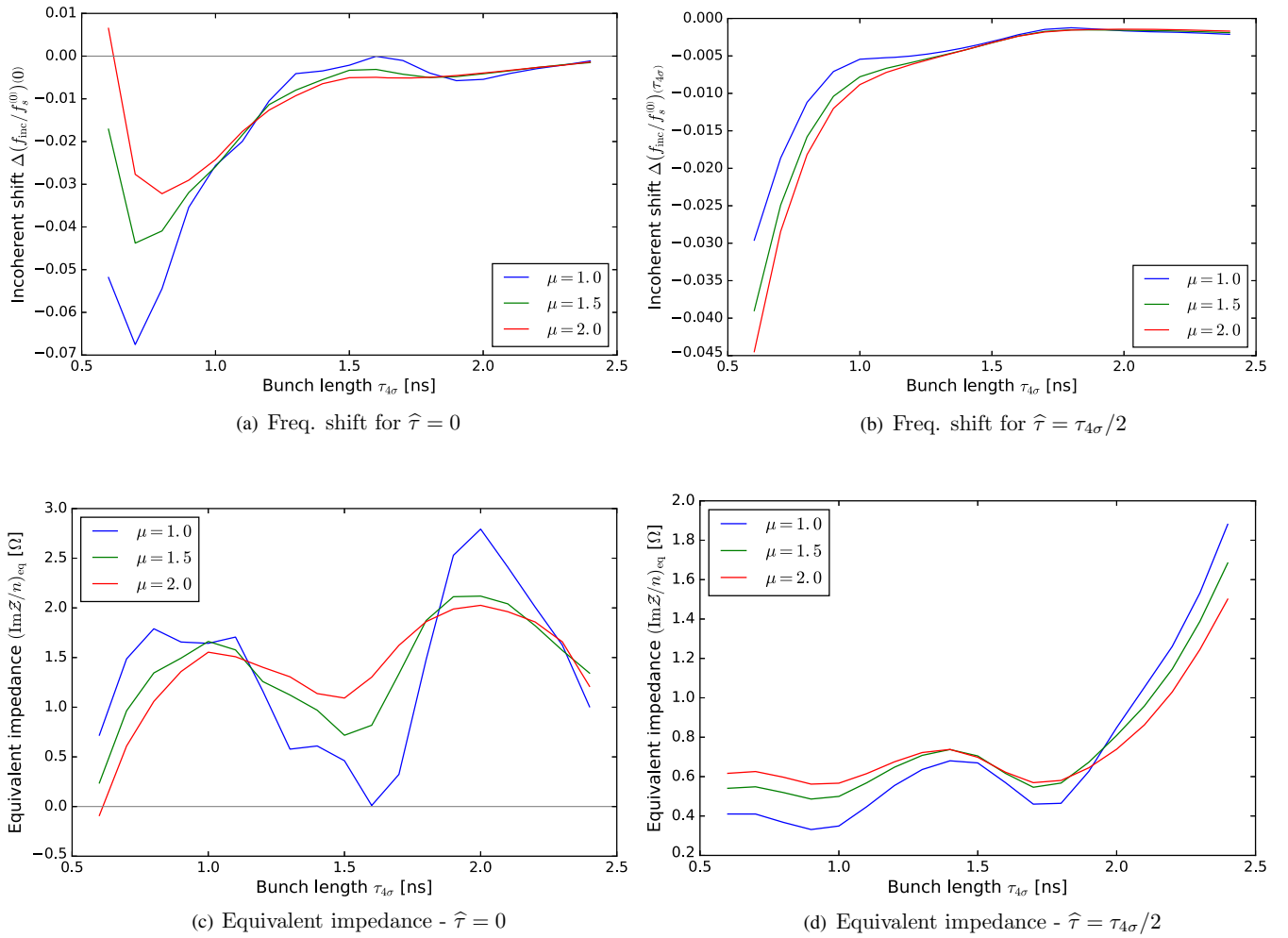


FIG. 8. The incoherent synchrotron frequency shift calculated for particle distributions with different μ as a function of the bunch length $\tau_{4\sigma}$, for the Q26 optics parameters and $N_b = 5 \times 10^{10}$ ppb using the full SPS impedance model. The upper plots correspond to the incoherent frequency shift for small (left) and large (right) particle oscillation amplitudes $\hat{\tau}$. The bottom plots (c) and (d) are the equivalent reactive impedances $(\text{Im}\mathcal{Z}/n)_{\text{eq}}$ corresponding to cases (a) and (b).

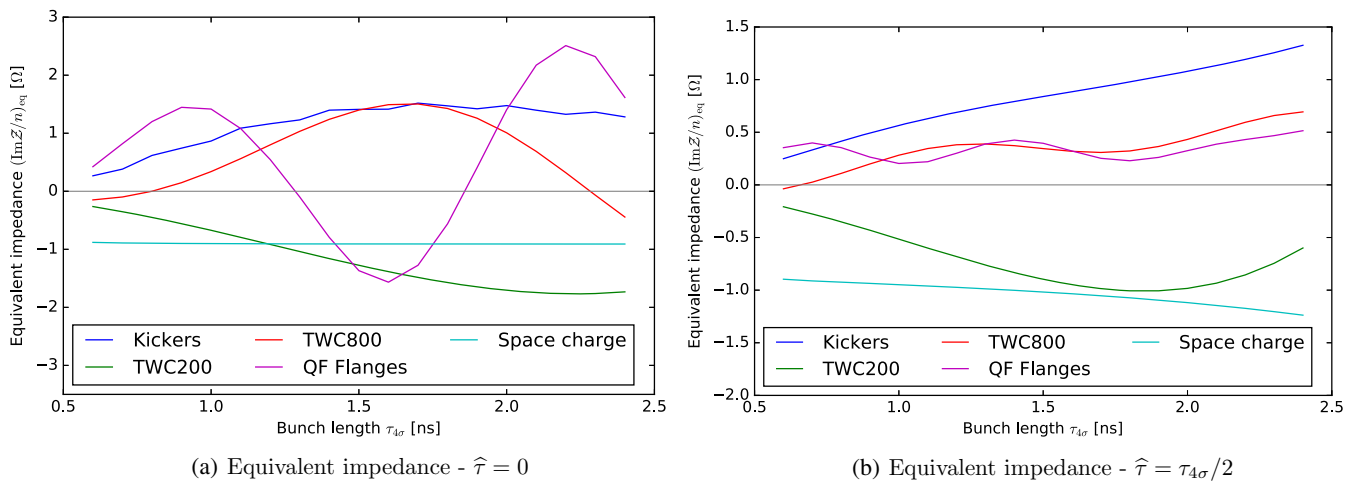


FIG. 9. The equivalent impedance $(\text{Im}\mathcal{Z}/n)_{\text{eq}}$ of the main SPS impedance sources (shown in Fig. 1), taken separately for a bunch distribution with $\mu = 1$, and for small (left) and large (right) particle oscillation amplitudes $\hat{\tau}$.

expected from the various SPS impedance sources. For example, the space charge effect is a constant capacitive impedance and as expected its equivalent impedance is constant with a negative sign in Fig. 6. Broad-band impedance sources (e.g. the kickers) give for both small and high amplitude $\hat{\tau}$ a contribution which is not strictly comparable to a constant impedance $\text{Im}\mathcal{Z}/n$, but which is weakly dependent on bunch length. The contribution from the TWC at 200 MHz in this bunch length range is capacitive. Finally, resonant impedances located at high frequencies (the TWC at 800 MHz and the vacuum flanges) give a more particular behavior with an important dependence on bunch length and particle oscillation amplitudes. For small amplitudes of oscillations they can either act as inductive or capacitive, depending on the bunch length, for small $\hat{\tau}$, while for large $\hat{\tau}$ they mainly act as an inductive impedance. They are the source of the variations in Fig. 8(c) and the peaks at $\tau_{4\sigma} \approx 0.7$ ns and $\tau_{4\sigma} \approx 1.4$ ns in Fig. 8(d).

C. Coherent synchrotron frequency shift

In addition to the incoherent shift due to the stationary bunch distribution, the synchrotron frequency is also shifted due to the bunch spectrum appearing from oscillations of mode m (coherent shift $\Delta f_{\text{coh},m}$). Like for the incoherent shift, the actual effect of the impedance depends on the overlapping of the perturbed bunch spectrum with the impedance and can be described by the effective impedance for coherent oscillations $\text{Im}\mathcal{Z}_{\text{coh},m}$. The coherent synchrotron frequency shift can be evaluated by solving the linearized Vlasov equation for small amplitudes of particle oscillation $\hat{\tau} \rightarrow 0$. Following these assumptions and for quadrupole oscillations $m = 2$, $\Delta f_{\text{coh},2}$ can be expressed as [9]:

$$\Delta f_{\text{coh},2} = \frac{3\Gamma(5/2)}{8\pi^{5/2}} \frac{q^2\eta}{\beta^2 E f_{s0,\text{inc}} \tau_L^3} \text{Im}\mathcal{Z}_{\text{coh},2} N_b, \quad (21)$$

where the effective impedance $\text{Im}\mathcal{Z}_{\text{coh},2}$ is

$$\text{Im}\mathcal{Z}_{\text{coh},2} = \frac{\sum_{n=-\infty}^{\infty} \mathcal{S}_2(n) (\text{Im}\mathcal{Z}/n)}{\sum_{n=-\infty}^{\infty} \mathcal{S}_2(n)}. \quad (22)$$

For a parabolic bunch distribution with $\mu = 1$, the perturbed spectrum of quadrupole oscillations can be described by [9]:

$$\mathcal{S}_2(f) = \frac{[J_{5/2}(2\pi f \tau_L)]}{2\pi f \tau_L}. \quad (23)$$

A first approximation consists in considering a constant $\text{Im}\mathcal{Z}/n$ in Eq. (22), giving $\text{Im}\mathcal{Z}_{\text{coh},2} = \text{Im}\mathcal{Z}/n$. Since the coherent shift $\Delta f_{\text{coh},2}$ scales $\propto 1/\tau_L^3$ like the incoherent shift Δf_{inc} , the ratio between the two does not depend on the bunch length and is

$$\frac{\Delta f_{\text{coh},2}}{2\Delta f_{\text{inc}}} \underset{\hat{\tau} \rightarrow 0}{\approx} -\frac{3\pi}{16} \frac{1}{(1 + \frac{\Delta f_{\text{inc}}}{f_{s0}})} \approx -0.6. \quad (24)$$

The coherent synchrotron frequency shift has an opposite sign and is comparable in amplitude with respect to the incoherent one. The total shift $2\Delta f_{\text{inc}} + \Delta f_{\text{coh},2}$ is reduced by more than a half with respect to the incoherent shift alone, as shown in Fig. 10(a). Next, the effective impedance $\text{Im}\mathcal{Z}_{\text{coh},2}$ is computed numerically using the full SPS impedance model and the influence of the coherent shift $\Delta f_{\text{coh},2}$ is shown in Fig. 10(b). Results are significantly

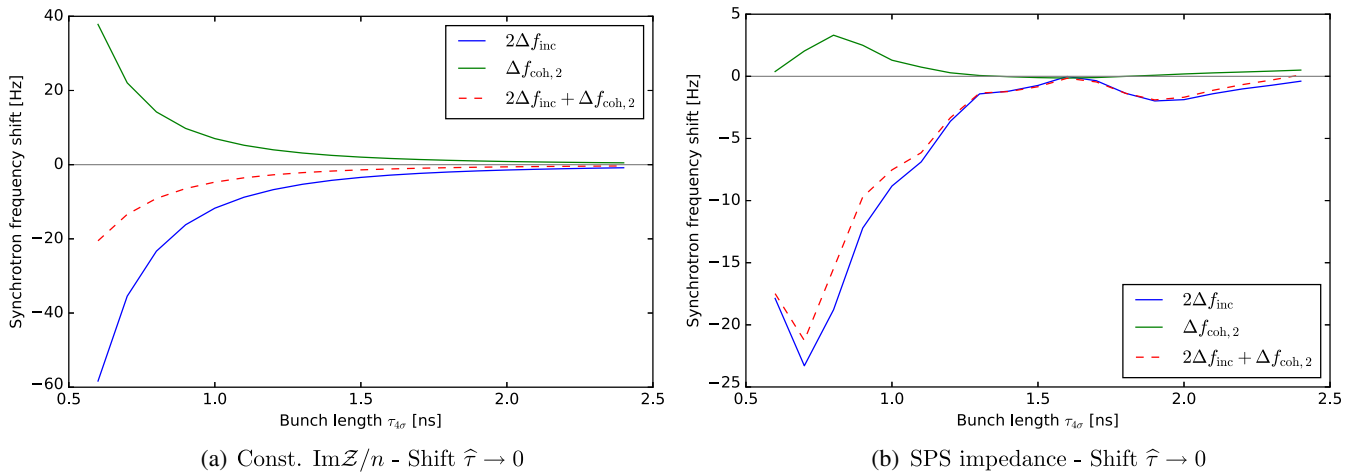


FIG. 10. Contribution of the incoherent shift $2\Delta f_{\text{inc}}$ and the coherent shift $\Delta f_{\text{coh},2}$ to the total synchrotron frequency shift $2\Delta f_{\text{inc}} + \Delta f_{\text{coh},2}$ as a function of bunch length, for a pure inductive impedance $\text{Im}\mathcal{Z}/n = 3 \Omega$ (left) and the full SPS impedance (right). The Q26 optics parameters in Table I were used with $N_b = 5 \times 10^{10}$ ppb.

different from the case with constant $\text{Im}\mathcal{Z}/n$ and the coherent shift is small in comparison to the incoherent one.

The definition of the effective impedance in Eq. (20) can be extended to include the coherent frequency shift $\Delta f_{\text{coh},2}$:

$$(\text{Im}\mathcal{Z}/n)_{\text{eq}} \stackrel{\text{def}}{=} \frac{\omega_{\text{rev}}^2 V_{\text{RF}} h}{6q} \frac{(\Delta f_{\text{inc}} + \Delta f_{\text{coh},2}/2)}{f_{s0}} \frac{\tau_{4\sigma}^3}{N_b}. \quad (25)$$

To understand better the influence of the various SPS impedance sources shown in Fig. 1, the equivalent impedance of each source was computed taking also into account the coherent shift $\Delta f_{\text{coh},2}$. Results are shown in Fig. 11 (dashed lines). For broadband impedance sources (e.g. space charge, kickers) the equivalent impedance is reduced by the coherent shift by more than a half regardless of the bunch length, as expected for impedance sources close to a constant $\text{Im}\mathcal{Z}/n$. Concerning the high frequency impedance sources (e.g., the TWC at 800 MHz, the vacuum flanges), the influence of the coherent shift is very small. Finally, for the TWC at 200 MHz the influence of the coherent shift $\Delta f_{\text{coh},2}$ depends on the bunch length. For small bunch length $\tau_{4\sigma} < 1.5$ ns the influence of $\Delta f_{\text{coh},2}$ is significant and reduces the equivalent impedance, while for large bunch length $\tau_{4\sigma} > 2.3$ ns the coherent shift even changes the sign and further increases the total shift.

To conclude, the quadrupole oscillation frequency f_{s2} is mainly determined by the particles oscillating with large oscillation amplitude \hat{v} . The observed shift with intensity is mainly defined by the incoherent synchrotron frequency shift Δf_{inc} , while for the SPS impedance the coherent shift $\Delta f_{\text{coh},2}$ is assumed to be negligible. The dependence of f_{s2} on the bunch length is very strong, due to both the nonlinearities of the rf bucket and the frequency dependence of the SPS impedance.

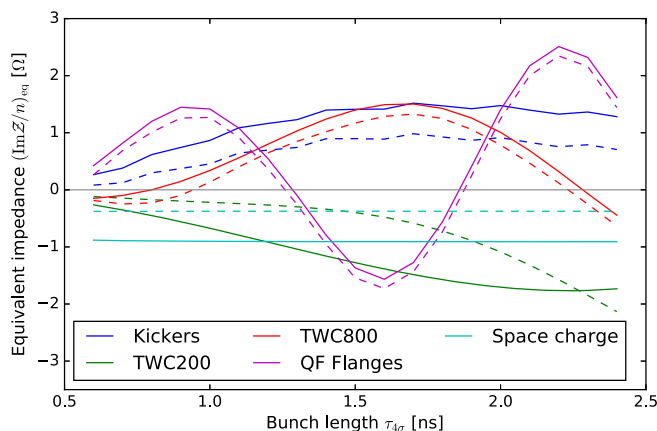


FIG. 11. The equivalent impedance $(\text{Im}\mathcal{Z}/n)_{\text{eq}}$ of the main SPS impedance sources in Fig. 1 taken separately. The solid lines correspond to the equivalent impedances defined only from the incoherent shift Δf_{inc} as in Fig. 9, the dashed lines correspond to the equivalent impedances taking also into account the coherent shift $\Delta f_{\text{coh},2}$.

III. MEASUREMENTS OF THE QUADRUPOLE FREQUENCY SHIFT

A. Setup

The quadrupole oscillation frequency f_{s2} was measured at injection in the SPS (kinetic energy $E_k = 25$ GeV) and its dependences, described in Sec. II, were analyzed by exploring a broad range of bunch intensities and lengths. The rf parameters in the SPS injectors were adjusted to scan the injected bunch properties [12]. In the SPS, the rf voltage was set for the injected bunch to be slightly mismatched hence initiating bunch length oscillations. The dipole oscillations were reduced thanks to the rf phase loop and this effect is considered negligible below. The longitudinal bunch profiles were acquired every turn using a wall current monitor for an amount of turns covering approximately ten quadrupole oscillations periods.

The bunch length in measurements is increased, mainly due to the perturbation from the cables connecting the wall current monitor with the oscilloscope. The modification of the bunch length from the wall current monitor is negligible, and the measured bunch profile is lengthened by 5%–10% by the cables transfer function. The lengthening comes from short coaxial cables in the measurement line, the main part of the cables consists of a long fiber optic link, which has a negligible impact on the measured bunch profile. The transfer functions of the wall current monitor and cables were measured, and the bunch profile was systematically corrected taking them into account [13,14].

The profiles were fitted with the binomial function (10) with $\mu = 3/2$ and the bunch length was defined as $\tau_{4\sigma} = 4\sigma_{\text{rms}}$, where σ_{rms} is the rms bunch length of the fitting profile. We note τ_{av} and $\Delta\tau$ corresponding to the average bunch length and the peak-to-peak amplitude of the bunch length oscillations. The frequency of the bunch length oscillations f_{s2} was obtained from the maximum component of the fast Fourier transform. The bunch intensity N_b was measured using a DC beam current transformer and an averaged value was taken. Finally, each acquired SPS cycle associates the quadrupole frequency f_{s2} with an average bunch length τ_{av} , a peak-to-peak amplitude of oscillations $\Delta\tau$ and a bunch intensity N_b . Examples of these acquisitions were shown in Fig. 2.

Two different optics are available in the SPS, named after the transverse tune: Q20 and Q26. The main difference is the different γ_t and therefore a different synchrotron frequency for the same bucket area \mathcal{A}_b . Another difference is the longitudinal space charge effect which is larger in the Q26 optics with respect to the Q20 optics. This is due to the different dispersion function which gives a smaller horizontal bunch size in the Q26 optics for the same transverse emittance [5]. Measurements were performed in both optics, and the raw data of the quadrupole frequency as a function of intensity and the average bunch length is

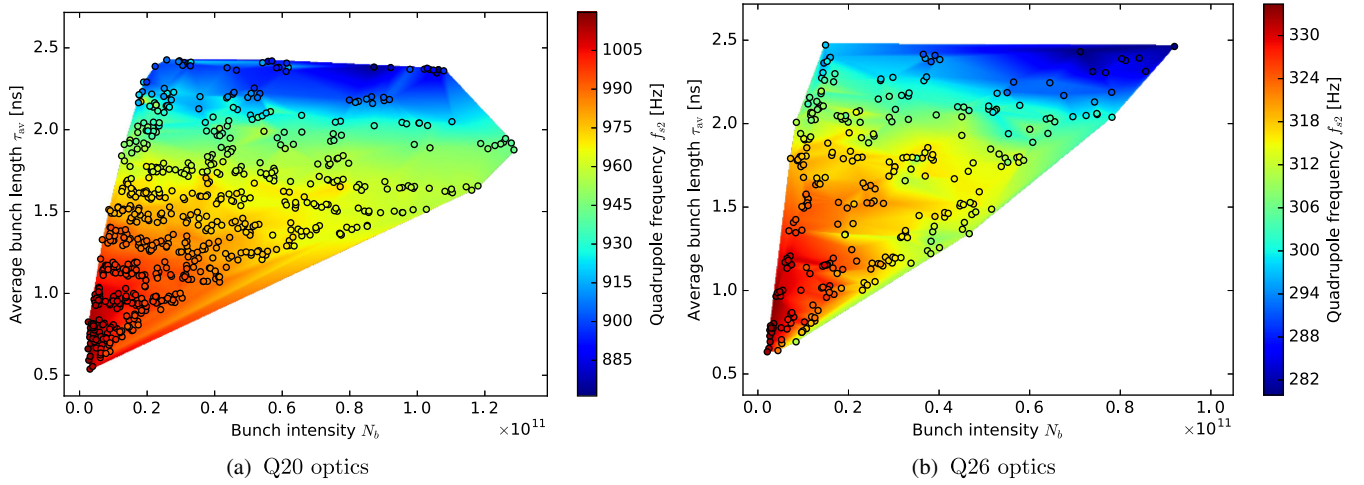


FIG. 12. Measured quadrupole frequency f_{s2} as a function of bunch length and intensity in both Q20 (left) and Q26 (right) optics. Each point corresponds to a single measurement, and the colored surface corresponds to the quadrupole frequency (gaps were filled using interpolation).

shown in Fig. 12. The corresponding beam and machine parameters are shown in Table I.

B. Data analysis and results

The dependence of the quadrupole frequency f_{s2} on intensity was studied by selecting the data with the same average bunch length τ_{av} (within ± 50 ps). For each set, the dependence on intensity is obtained from the fit by a linear function $f_{s2} = a + bN_b$, as expected from Eq. (19). The origin of the fit a corresponds to the quadrupole frequency without intensity effects, while the slope b contains the information about the reactive impedance. Examples of measured quadrupole frequency f_{s2} as a function of intensity for different sets of average bunch length τ_{av} together with fits are shown in Fig. 13.

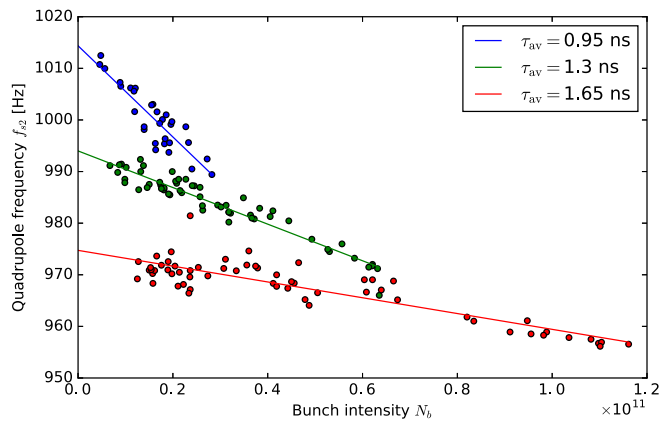


FIG. 13. Examples of measured quadrupole frequency f_{s2} as a function of intensity for selected average bunch lengths τ_{av} (within ± 50 ps) in the Q20 optics. The lines correspond to a linear fit.

The dependence of the quadrupole frequency on bunch length can be studied from the fitted parameters a and b obtained for each set of τ_{av} . As discussed in Sec. II, the measured quadrupole oscillations are mainly performed by the mismatched particles from the outer part of the distribution. The first consequence is that the quadrupole frequency without intensity effects $a(\tau_{av})$ should follow Eq. (4). The comparison of measurements with the expected analytical formula is shown in Figs. 14(a) and 14(b) for both optics. They are in good agreement, confirming that the measured quadrupole frequency is dominated by contributions from particles with large synchrotron oscillation amplitudes. The small discrepancy between measurements and the expected scaling comes from the fact that Eq. (4) is valid for particles with maximum oscillation amplitude, while in measurements the frequency is determined by the sum of all the particles defining the mismatch.

It is possible to extrapolate the value of $2f_{s0}$ from the measured $a(\tau_{av} \rightarrow 0)$ which gives the actual amplitude of the rf voltage during measurements (this parameter has an uncertainty of $\approx 5\%$). For both Q20 and Q26 optics the measured values ($2f_{s0} \approx 1035$ Hz in the Q20 optics and $2f_{s0} \approx 342$ Hz in the Q26 optics) are in good agreement with the expected values shown in Table I. The measured slope b is shown in Figs. 14(c) and 14(d) and it scales approximately as $\propto 1/\tau_{av}^3$, in accordance to the expected scaling of the synchrotron frequency shift for large particle oscillation amplitudes $\hat{\tau}$ [see Fig. 8(b)].

In previous studies of the synchrotron frequency shift as a probe of the reactive impedance, only the slope b was taken to compare measurements and simulations. However, the strong dependence of the slope b on bunch length implies that small deviations in the measured bunch length could lead to significant difference between measurements

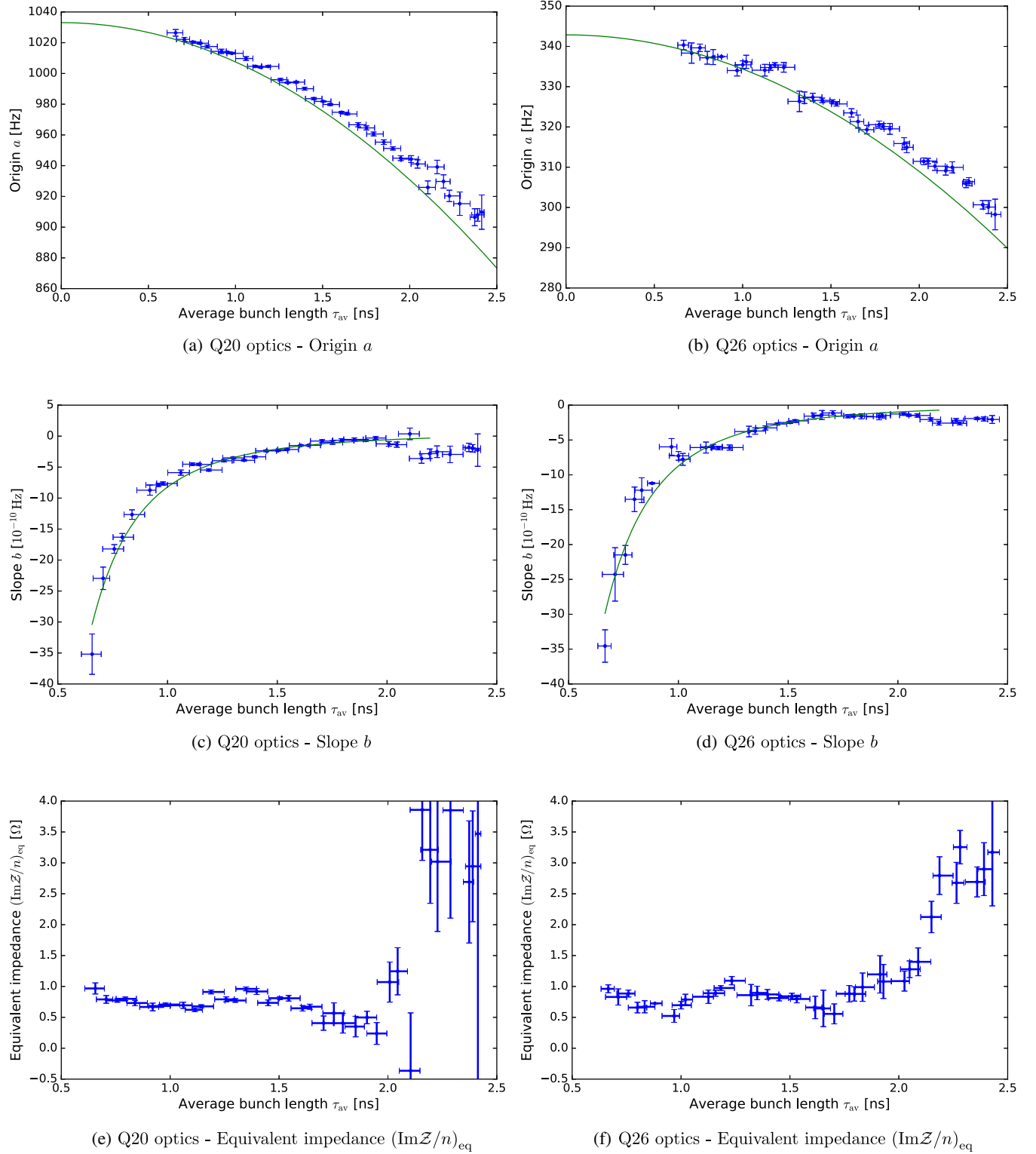


FIG. 14. The fitted origin a (top), slope b (middle) and their expected scaling (green), from Eqs. (4) and (19). The Eq. (26) was used to obtain the corresponding equivalent impedance $(\text{Im}Z/n)_{eq}$ (bottom) of the quadrupole frequency shift with intensity, as a function of the average bunch length τ_{av} , in the Q20 (left) and Q26 (right) optics.

and simulations (e.g., due to systematic error in the measured profile from the measurement line, see III A). Therefore, it is helpful to use as a figure of merit the equivalent impedance with less strong dependence on bunch length. The analyzed parameters $a = 2f_s^{(0)}$ and $b = -2\Delta f_{\text{inc}}/N_b$ are recombined to obtain the equivalent reactive impedance as:

$$(\text{Im}\mathcal{Z}/n)_{\text{eq}} = \frac{\omega_{\text{rev}}^2 V_{\text{RF}} h b}{6q a} \tau_{\text{av}}^3, \quad (26)$$

following the same assumptions as used to derive Eq. (19). The results are shown in Figs. 14(e) and 14(f). A remarkable observation is that measured pattern matches very well the results obtained semianalytically and shown in Fig. 8(d). The values of $(\text{Im}\mathcal{Z}/n)_{\text{eq}}$ are also very close, although the two quantities are not directly comparable as Eq. (19) is derived for a single particle. Moreover, a parabolic bunch profile was assumed in calculations while in measurements it varies a lot. Nevertheless, the relative agreement shows that in measurements the incoherent frequency shift for particles with large oscillation amplitudes $\hat{\tau}$ is indeed the dominant effect (assuming also that the impedance model is close enough to reality). Further details will be studied below from the comparison with macro-particle simulations. Note that the equivalent impedances $(\text{Im}\mathcal{Z}/n)_{\text{eq}}$ are very similar for the Q20 and Q26 optics since the dependence on the machine parameters V_{RF} and η was removed.

For the measured equivalent impedance $(\text{Im}\mathcal{Z}/n)_{\text{eq}}$ we can distinguish three different bunch length intervals. For $\tau_{\text{av}} < 1.7$ ns, the results are similar in pattern and value between the Q20 and Q26 optics and correspond to the ideal bunch length range for these measurements. At $\tau_{\text{av}} \approx 1.7$ ns, the measured equivalent impedance $(\text{Im}\mathcal{Z}/n)_{\text{eq}}$ in the Q20 and Q26 optics starts to be different. For the Q20 optics, the measured values keeps decreasing increase whilst the equivalent impedance grows in the case of the Q26 optics. For $\tau_{\text{av}} > 2$ ns the measured equivalent impedance $(\text{Im}\mathcal{Z}/n)_{\text{eq}}$ in Q20 is completely unusable. This is explained by the motion of a mismatched bunch in phase space which is heavily affected by the nonlinearities of the rf bucket for large bunch lengths. As shown in Fig. 2, the consequence is that the bunch profile changes with time and bunch length oscillations are quickly damped due to filamentation. In addition, the bunch is shortened in the SPS injector (PS) by a fast rf voltage increase (bunch rotation in phase space). For large bunch lengths, the distribution in phase space is distorted during the bunch rotation in the longitudinal phase space and has an ‘‘S-shape’’ [15], making the filamentation effects even more difficult to reproduce. Moreover, the spectrum of a filamenting bunch has components at high frequency, which could affect the synchrotron frequency shift. In those

conditions the results are varying from one acquisition to another. Nevertheless, the main observation is that for large bunch lengths the equivalent impedance $(\text{Im}\mathcal{Z}/n)_{\text{eq}}$ for $\tau_{\text{av}} > 2$ ns is increasing, implying that long bunches are mainly sampling inductive impedance as expected from Fig. 8(d).

IV. PARTICLE SIMULATIONS

A. BLOND simulations

The dependence of the quadrupole frequency shift on the SPS impedance can be studied more precisely by macro-particle simulations that include the rf non-linearities and induced voltage. The simulation code BLOND was written at CERN to simulate longitudinal beam dynamics in synchrotrons and was successfully benchmarked with measurements in various accelerators and physics cases, including the synchrotron frequency shift with intensity [16]. All simulations were done using the SPS impedance model presented in Fig. 1 (both resistive and reactive parts).

The SPS machine parameters were set in simulations to be the same as in measurements (for both optics in Table I). To cover the same range of longitudinal emittances and bunch intensities obtained in measurements, each acquisition was reproduced in simulations by taking the injected bunch profile and reconstructing the bunch distribution in phase space using the Abel transform [17]. To get in simulations a mismatch close to the one in measurements, the bunch distribution in phase space was generated and the energy spread was iteratively adjusted so that the peak-to-peak bunch length oscillations $\Delta\tau$ are similar to the corresponding acquisition. For small bunch lengths, this approach is good enough to get input distributions close to the ones extracted from the PS without having to simulate the bunch rotation in the PS. Simulation results analyzed applying exactly the same method as used for measurements are presented in Fig. 15.

Overall, simulations using the present SPS impedance model are in good agreement with measurements and the nontrivial dependence of the equivalent impedance $(\text{Im}\mathcal{Z}/n)_{\text{eq}}$ on bunch length is well reproduced in both optics. Nevertheless, some systematic deviations can be noticed. First, the equivalent impedance $(\text{Im}\mathcal{Z}/n)_{\text{eq}}$ is in general lower in simulations than in measurements, suggesting that some impedance is still missing in the SPS impedance model. Next, the discrepancy is higher for $\tau_{\text{av}} \approx 1.6$ ns, indicating that the missing impedance has a particular frequency dependence. The results for $\tau_{\text{av}} > 1.7$ ns are less accurate due to the limitations described above and may not be suitable to draw reliable assumptions on possible missing impedance.

One expects that the machine impedance does not depend on the optics. However, the measured variations of the equivalent impedance as a function of the average bunch length τ_{av} are larger in the Q26 optics than in the

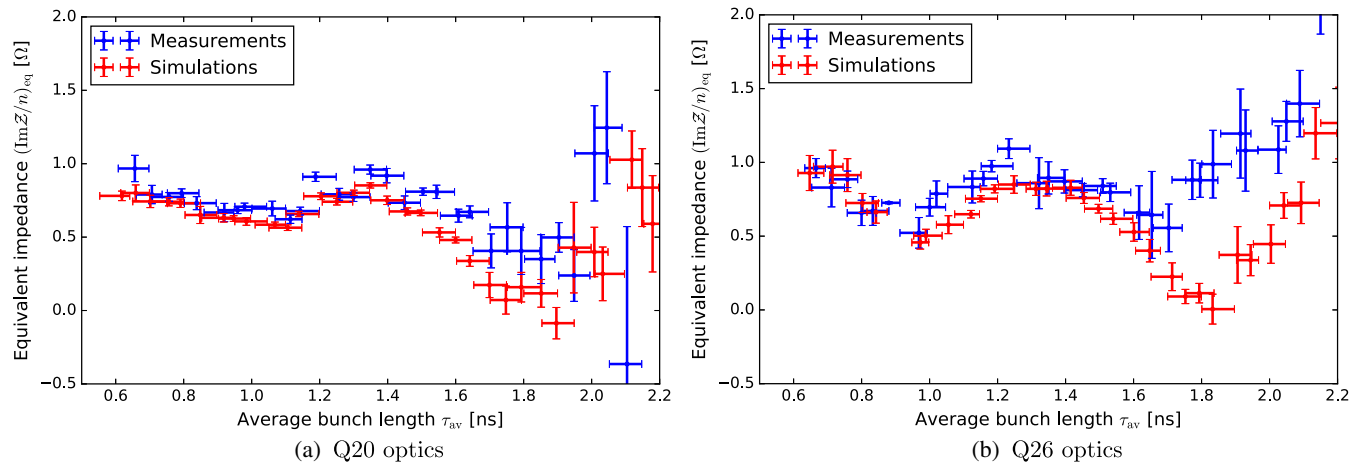


FIG. 15. Equivalent impedance $(\text{Im}\mathcal{Z}/n)_{\text{eq}}$ as a function of bunch length obtained from measurements (blue) and simulations (red) using the full SPS impedance model in the Q20 (left) and Q26 (right) optics.

Q20. In the two optics measurements were done with the same (maximum) range of bunch intensity and longitudinal emittances, determined by the abilities of the SPS injectors. To get the same degree of mismatch for the injected bunches (bucket area) in both optics, the rf voltage in the Q20 optics was set to a higher value (see Table I). Then, the relative amplitude of the induced voltage to the rf voltage is higher in the Q26 optics. Therefore, for bunches with the same intensity and length, the effect of potential well distortion and nonlinear terms in Eq. (6) and beyond are more significant in the Q26 optics. To get the same measured equivalent impedance, measurements in the Q20 optics should have been done with higher bunch intensities for the same range of longitudinal emittance, in order to get the same relative synchrotron frequency shift $\Delta f_{\text{inc}}/f_s^{(0)}$. However, these bunch parameters are not achievable in the SPS injectors. Nevertheless, the bigger variations of the equivalent impedance as a function of the average bunch length τ_{av} in the Q26 optics are reproduced in particle simulations.

B. Evaluation of the missing impedance

To define possible missing impedance sources, the simulations were reiterated by adding a variable amount of constant inductive impedance $\text{Im}\mathcal{Z}/n$. Results are shown in Fig. 16. The present SPS impedance including space charge is represented in blue and the deviations between measurements and simulations could be explained by an additional inductive impedance in the order of $\text{Im}\mathcal{Z}/n \approx (0 - 1.5) \Omega$ depending on the bunch length. This is comparable to the longitudinal space charge impedance of $(\text{Im}\mathcal{Z}/n)_{\text{SC}} \approx -1 \Omega$. Omitting the longitudinal space charge impedance in simulations would correspond to the red line. In this case, the interpretation would have been opposite, since we would have concluded that the inductive impedance in the present model is in excess. Therefore, the

longitudinal space charge effects are indeed not negligible and should be included in simulations at flat bottom in the SPS. An accurate evaluation of the longitudinal space charge impedance was done [5], leading to the values shown in Table I for both optics.

By using the previous scan in simulations adding a variable amount of constant inductive impedance $\text{Im}\mathcal{Z}/n$, it is possible to determine for each bunch length the necessary impedance value to reach a perfect agreement between simulations and measurements. Results are shown in Fig. 17 for both optics.

For $\tau_{\text{av}} < 1.4$ ns, it is necessary to add $\Delta(\text{Im}\mathcal{Z}/n) \approx 0.3 \Omega$ in the Q20 optics and $\Delta(\text{Im}\mathcal{Z}/n) \approx 0.5 \Omega$ in the Q26 optics to remove the deviations. For this large range of bunch lengths, a broadband impedance source could be the missing contribution, as determined in the previous section. Whilst non-negligible, this missing contribution is still small in comparison with the full impedance budget and

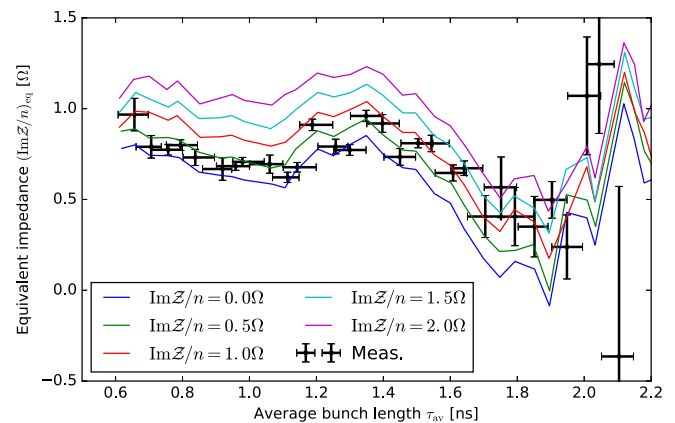


FIG. 16. Measured equivalent impedance $(\text{Im}\mathcal{Z}/n)_{\text{eq}}$ (black) in the Q20 optics compared with simulations (colored lines) adding a variable amount of inductive impedance in the range $\text{Im}\mathcal{Z}/n = (0 - 2) \Omega$ to the full SPS impedance model.

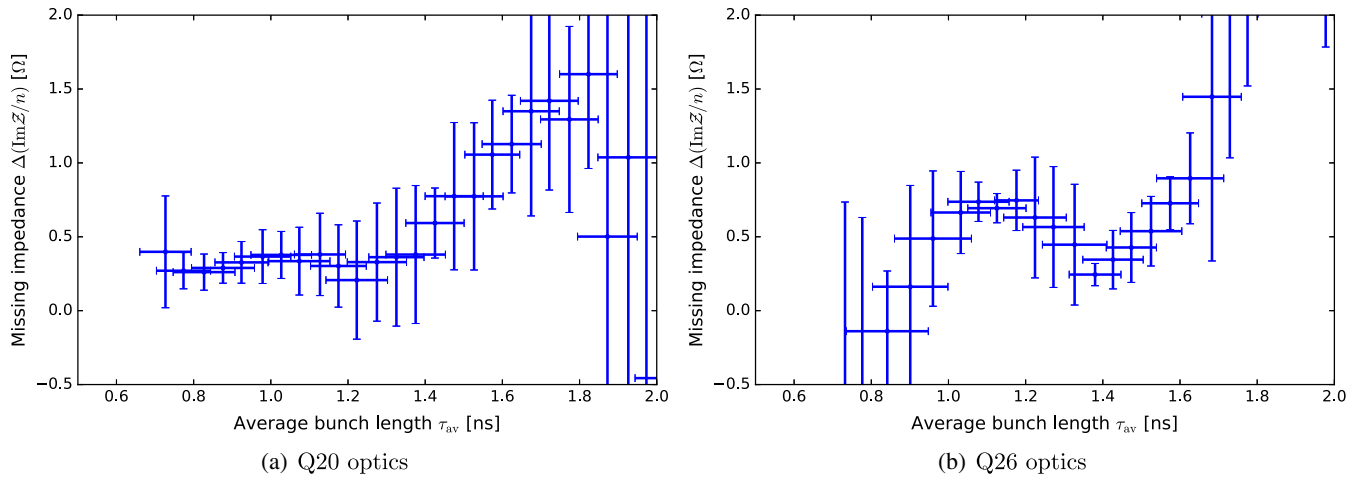


FIG. 17. Missing inductive impedance $\text{Im}Z/n$ as a function of bunch length needed to get a perfect agreement between measurements and simulations shown in Fig. 15 for both Q20 (left) and Q26 (right) optics.

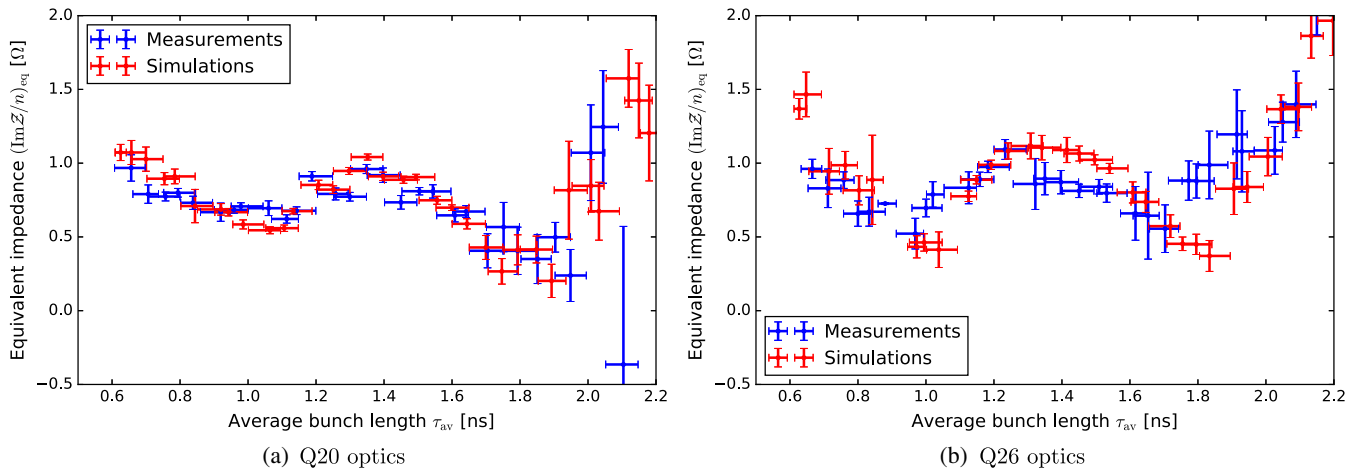


FIG. 18. Equivalent impedance $(\text{Im}Z/n)_{\text{eq}}$ in measurements and simulations after adding an extra resonator with $f_r = 350$ MHz, $R/Q = 3$ k Ω and $Q = 1$ to the SPS impedance model to compensate for deviations from measurements in both Q20 (left) and Q26 (right) optics.

could be explained by an underestimation of a source in the model or some contributions that were not yet included.

For τ_{av} in the range (1.4–1.7) ns, the missing impedance is increasing linearly, suggesting that an impedance source as a resonator could also be missing, as shown in Sec. II. Simulations were done with an additional resonator and its resonant frequency f_r and impedance R/Q were scanned to further reduce the discrepancy (with $Q = 1$). The best agreement was found for a resonator with $f_r \approx (350 \pm 50)$ MHz and $R/Q \approx (3 \pm 1)$ k Ω , leading to an almost perfect agreement in the Q20 optics as shown in Fig. 18(a). While in the Q26 optics the agreement is also improved, some small deviations are still present at $\tau_{\text{av}} \approx 1.0$ ns and $\tau_{\text{av}} \approx 1.5$ ns [see Fig. 18(b)]. Adding a single resonator is most probably not enough to correct all the deviations between measurements and simulations. A perfect

description of the missing impedance is a multiparametric task which requires a very large amount of measured data with small error bars. Moreover, the realistic frequency dependence of a device contributing to the machine impedance could be more complex than that of a single resonator. Nevertheless, clear indications for the missing effective impedance as a function of bunch length can be exploited to get hint and direction for further searches. The missing contribution, depending on its frequency, could also be critical to have a reliable SPS impedance model for the bunch stability studies required for the SPS upgrade.

V. CONCLUSIONS

The measured quadrupole frequency shift with intensity has been used to probe the reactive part of the SPS machine impedance. Being very sensitive to the average bunch

length because of the nonlinearities of the rf bucket and the induced voltage, this method can nevertheless be used to have an estimate of the missing impedance and its frequency dependence. Measurements were done in the SPS in two different optics and allowed, from good agreement with particle simulations, to show that the present SPS impedance model is satisfactory to reproduce the measured synchrotron frequency shift. The agreement can be further increased by adding a resonant impedance at $f_r \approx 350$ MHz with $R/Q \approx 3$ k Ω and $Q = 1$, the real source to be investigated. As the studies for the HL-LHC project rely on the accurate reproduction of beam instabilities, any missing impedance could be crucial and this method is an effective way to test the existing impedance model. Beyond the evaluation of the longitudinal impedance model, the study of the synchrotron frequency shift is also important as it is a key component to determine the instability mechanisms related to the loss of Landau damping.

ACKNOWLEDGMENTS

We would like to thank the impedance working group at CERN for the development of the SPS impedance model and in particular J. Varela, C. Zannini, and B. Salvant. We would also like to thank T. Bohl for helping during the measurements in the SPS and S. Hancock for the help in the preparation of the necessary cycles in the PSB and PS. We are grateful to the MD coordinators for providing with beam time and the operation team for setting up the cycles. Finally we would like to thank BLOND developers for their contributions to the simulation code.

-
- [1] G. Apollinari, I. Béjar Alonso, O. Brüning, M. Lamont, and L. Rossi, CERN Report No. CERN-2015-005, 2015.
 - [2] H. Damerau, A. Funken, R. Garoby, S. Gilardoni, B. Goddard, K. Hanke, A. Lombardi, D. Manglunki, M. Meddahi, B. Mikulec, G. Rumolo, E. Shaposhnikova, M. Vretenar, and J. Coupard, CERN Report No. CERN-ACC-2014-0337, 2014.
 - [3] J.E. Campelo, T. Argyropoulos, T. Bohl, F. Caspers, J. Esteban Müller, J. Ghini, A. Lasheen, D. Quartullo,

- B. Salvant, E. Shaposhnikova, and C. Zannini, An extended SPS longitudinal impedance model, in *Proceedings of IPAC2015, Richmond, VA* (JACoW, Geneva, 2015), MOPJE035, pp. 360–362.
- [4] J.E. Campelo, Longitudinal impedance characterization of the CERN SPS vacuum flanges, in *Proceedings of IPAC2015, Richmond, VA* (JACoW, Geneva, 2015), MOPJE036, pp. 363–365.
- [5] A. Lasheen, Report No. CERN-ACC-NOTE-2016-0074, 2016.
- [6] E. Shaposhnikova, T. Bohl, and T. Linnecar, Longitudinal peak detected schottky spectrum, in *Proceedings of HB2010, Morschach* (JACoW, Geneva, 2010), TUO1C04, pp. 363–367.
- [7] M. Blaskiewicz, J. Brennan, and K. Mernick, Longitudinal impedance of RHIC, in *Proceedings of IPAC2015, Richmond, VA* (JACoW, Geneva, 2015), MOPMN020, pp. 746–747.
- [8] J.L. Laclare, Bunched beam coherent instabilities, in *Proceedings of CAS 1985, Geneva, Switzerland*, Vol. I (CERN, Geneva, 1987), pp. 264–326.
- [9] A.W. Chao, *Physics of Collective Beam Instabilities in High Energy Accelerators* (Wiley, New York, 1993).
- [10] E. Shaposhnikova, T. Bohl, H. Damerau, K. Hanke, T. Linnecar, B. Mikulec, J. Tan, and J. Tückmantel, Reference measurements of the longitudinal impedance in the CERN SPS, in *Proceedings of the 23rd Particle Accelerator Conference, Vancouver, Canada, 2009* (JACoW, Geneva, 2009), FR5RFP056, pp. 4667–4669.
- [11] K. Ng, *Physics of Intensity Dependent Beam Instabilities* (World Scientific, Singapore, 2005).
- [12] S. Hancock, CERN Report No. CERN-ATS-Note-2013-040 MD, 2013.
- [13] T. Bohl, CERN Report No. Note-2006-37, 2006.
- [14] T. Bohl, CERN Report No. Note-2011-09, 2011.
- [15] H. Timko, T. Argyropoulos, T. Bohl, H. Damerau, J.F. Esteban Müller, S. Hancock, and E. Shaposhnikova, Longitudinal transfer of rotated bunches in the CERN injectors, *Phys. Rev. ST Accel. Beams* **16**, 051004 (2013).
- [16] H. Timko, J.E. Müller, A. Lasheen, and D. Quartullo, Benchmarking the beam longitudinal dynamics code BLOND, in *Proceedings of International Particle Accelerator Conference (IPAC'16), Busan, Korea, 2016* (JACoW, Geneva, Switzerland, 2016), pp. 3094–3097.
- [17] P.W. Kreml, CERN Report No. MPS/Int. BR/74-1, 1974.